ORIGINAL

CrossMark

Numerical investigation of efficiency and economic analysis of an evacuated U-tube solar collector with different nanofluids

Hüseyin Kaya[1,2] • Kamil Arslan[1]

Abstract

In this paper, an evacuated U-tube tube solar collector (EUSC) was designed and simulated numerically. The thermal performance of the EUSC was analyzed under different operating conditions. In order to enhance the heat transfer efficiency and also collector efficiency, higher thermal conductivity working fluids were used. Ag, ZnO and MgO nanoparticles in 30%:70% (by volume) ethylene glycol-pure water (EG-PW) mixture and different nanoparticle volumetric concentrations were used as working fluids. The highest collector efficiency is found at 68.7% for 4.0 vol% Ag/EG-PW nanofluid which is 26.7% higher than EG–PW. Furthermore, using nanofluids in solar collectors helps to reduce the coal usage with CO_2 and SO_2 generation. The maximum values of reduction of coal usage and CO_2 and SO_2 generation are 855.5 kg, 2241.4 kg and 7.2 kg per year, respectively, when 30 solar collectors are installed with using 4.0 vol% Ag/EG-PW nanofluid. These findings reveal that the using of solar energy comprehensively is more beneficial for health of earth.

1 Introduction

Solar energy is the one of the most important and abundant renewable and clear resource for earth. Solar collectors are very significant devices that convert the radiation energy absorbed from the sun into usable energy. Today, heating water and generating electricity applications can be performed by using solar collectors and also in heating and cooling applications [1]. Fossil fuels have adverse effect for environment and these types of fuels will be depleted ultimately. For this reason, solar energy is becoming more important day by day. Therefore, many researchers have attributed great importance on developing thermal performance of solar energy systems. Evacuated tube solar collectors (ETSC) show better performance at higher temperatures (above 80 °C) and cold climates compared to flat plate ones. Moreover, higher thermal performance can be obtained by the reason of selective coating, availability of vacuum insulation which prevent from convective heat losses and cylindrical shape of the absorber part [2, 3]

Thus, the evacuated tube solar collectors are commonly used for solar thermal utilization in order to provide either hot water or space heating especially in residential applications including heat pipe and U-tube solar collectors.

In recent years, the developments in nanotechnology have enabled producing of nanofluids which are obtained with suspending of nanoparticles having sizes smaller than 100 nm into the conventional heat transfer fluids such as water, oil and ethylene glycol. In this way, improvement of thermophysical properties of heat transfer fluid, improves the heat transfer characteristics. It was seen from the past studies that conduction heat transfer capabilities of nanofluids were in high quantities [4–7]. Therefore, it has recently started to be done research on usability of nanofluids on different engineering applications. Because of the high heat transfer performance, it has been suggested to be used of nanofluids as a working fluid in solar collectors which are important in engineering applications. Because, the most important way of improving the efficiency of the evacuated tube solar collectors is to increase the solar radiation absorption capacity of the working fluid in the collectors [8–12].

Recently there are numerous studies about purposing nanofluids as collector working fluids in flat plate solar collectors. Yousefi et al. [8] made experiments in order to analyze the thermal behavior of Al_2O_3/water nanofluid to obtain thermal efficiency of a flat plate solar collector (FPSC) with with 0.2 and 0.4% weight fractions. They obtained a great enhancement in thermal efficiency (28.3%) at 0.2% nanofluid weight

✉ Hüseyin Kaya
   hkaya@bartin.edu.tr

1   Department of Mechanical Engineering, Karabük University, Karabük, Turkey

2   Department of Mechanical Engineering, Faculty of Engineering, Bartın University, 74100 Bartın, Turkey

Springer

fraction. In addition, another experimental study was conducted by Yousefi et al. [9] about using MWCNT/water nanofluid in a FPSC. The highest efficiency was obtained 0.4 wt% with respect to 0.2 wt%. Colangelo et al. [13] indicated that the heat transfer performance of a flat plate collector have been enhanced by 25% due to reduce of sedimentation of Al_2O_3/water nanofluid. Moghadam et al. [14] carried out an experimental study for determining the effects of CuO/water nanofluid on efficiency of a flat plate collector. It was obtained 21.8% increment in collector efficiency at 0.4% volume concentration and 1 kg/min mass flow rate with 40 nm nanoparticle size. Faizal et al. [15] made an analysis about size reduction of a flat plate solar collector using MWCNT nanofluids. It was reported that 37% size reduction took place in the original size of the collector. Mahian et al. [16] performed an analytical analysis for a mini-channel based flat plate solar collector for Cu/water, Al_2O_3/water, TiO_2/water, and SiO_2/water nanofluids. The calculations were carried out for up to 4.0% volume concentration and 25 nm nanoparticle size.

Several studies have been conducted about thermal performance of different types evacuated tube solar collectors. All glass, heat pipe and U-tube ETSC were numerically and experimentally investigated by many researchers [17–24]. Yin et al. [25] carried out an experimental study which can be regarded as one of the milestones for the testing of evacuated U-tube solar collectors. In this analysis, where pure water is used as the working fluid, the efficiency of the collector was determined under different operating conditions (ambient temperature, inlet temperature, mass flow rate, solar radiation intensity etc.). The thermal conductivity of the working fluid a solar collector plays vital role on the thermal efficiency. Exploiting from remarkable thermal conductivity of nanofluids is very advantageous to enhance the solar collector efficiency. Hence the nanoscience is very important for energy conversion technology and systems.

Liu et al. [26] experimentally analyzed an ETSC with an open thermosiphon using CuO/water nanofluid with 50 nm nanoparticle size and 1.2 wt%. They reported that the enhancement in maximum and mean efficiency are 6.6 and 12.4%, respectively. An experimental study was carried out by Kim et al. [27] about thermal efficiency of a EUSC by using Al_2O_3/water nanofluid as a working fluid with different nanoparticle sizes and volumetric concentrations. The highest efficiency was obtained at 1.0% volumetric concentration and 20 nm nanoparticle size by comparing with water. They have reported 72.4% as a highest collector efficiency for equal nanofluid concentrations. Tong et al. [28] made an theoretical study in order to comparing of EUSC and evacuated heat pipe solar collector. It was indicated that the heat pipe collector shows better performance than EUSC with 8% in efficiency in sunny day. However, EUSC overtaken heat pipe collector in stability and thermal performance in cloudy days.

Numerous studies have been carried out about analysis of enhancement of solar collector performance by using various nanofluids as working fluids as indicated above. Most of these studies are about only FPSC. Researches about performance of EUSC using nanofluids are very limited. Studies on the effects of nanofluid and base fluid concentrations in EUSC under various operating conditions on the thermal performance are also rare. Primary purpose of this paper is to investigate numerically the efficiency of a EUSC used Ag/EG-PW, ZnO/EG-PW and MgO/EG-PW nanofluids at different volumetric concentrations (1.0%, 2.0%, 3.0 and 4.0%) under same operating conditions. In addition, the effect of mass flow rate and heat losses on thermal efficiency are determined. The results of evaluations for thermal efficiency were compared with different types of nanofluids and the base fluid (EG-PW).

2 Modelling of solar collector

Evacuated tubes are composed of nested two glass tube manufactured high quality borosilicate. The U-type evacuated tube solar collectors work based on direct circulation method. These types of collectors include copper pipe networks in the evacuated tubes. Copper pipe collects the heat flux coming from the sun by entering in the evacuated tube and leaving from the tube. Therefore, there are cold inlet and hot outlet in each tube. The heat collector used in these types of tubes has supported with aluminum fin. This situation provides that more heat collection by copper with reducing the amount of air in the collector tube and increase conductive surface.

It is known that total solar radiation intensity from the sun is not absorbed completely from the solar collector because of the transmissivity and reflectivity. Therefore, optical efficiency must be taken into account for thermal efficiency calculations. Optical efficiency can be defined as the ratio of received solar radiation through its surface to appropriate solar resource. It is a function of the absorptivity (α) of the absorber, the transmissivity (τ) of the glass cover and the reflectivity (ρ) of the reflector.

Numerical investigation of thermal performance of a EUSC was made in this study by using necessary boundary conditions. As shown in Fig. 3, evacuated tubes are consisted of nested two glass tube manufactured high quality borosilicate and a U-tube is placed in the vacuum tubes in these types of solar collectors. Heat transfer takes place effectively because of the vacuum existence and this provides reduction of heat loss due to conduction, convection and radiation. It is possible to transfer the solar radiation to the working fluid with about 80% of solar radiation by passing the outer glass tube and tube coated by selective coating [3]. This is related with optical efficiency of an EUSC. In order to simplify the

calculations there are some assumptions: It is assumed that the overall heat transfer coefficient from the header tube is constant in the simulation and the influence of convection due to the air in the evacuated tube is negligible. Also all the processes in the solar collector are taken into account steady-state condition [29]. Net useful energy gain strongly influenced by energy losses from the absorber due to both convective heat losses to ambient and radiative heat losses to the environment. Hence overall heat loss coefficient should be determined for efficiency calculation accurately. A schematically representation of thermal resistances is used for calculating overall loss coefficient and describing the physical meaning as seen in Fig. 1. The resistances R_4 and R_7 are very small thus they are negligible.

The collected useful heat energy from the solar collector can be obtained from the difference of heat energy gained from the collector and the heat loss to the ambient. Also,
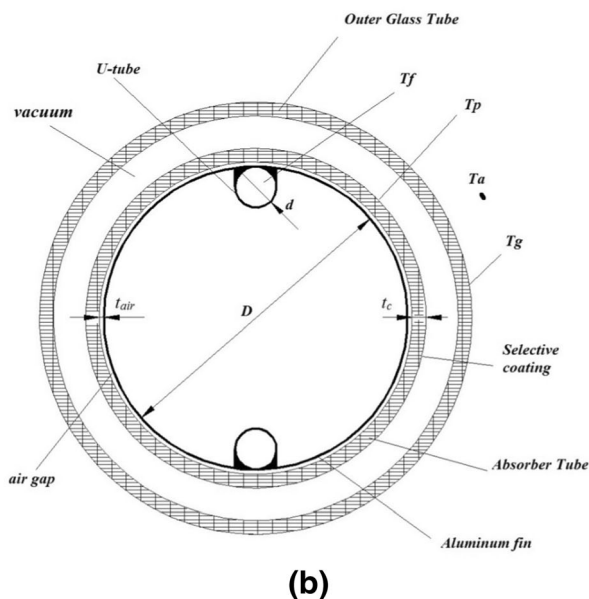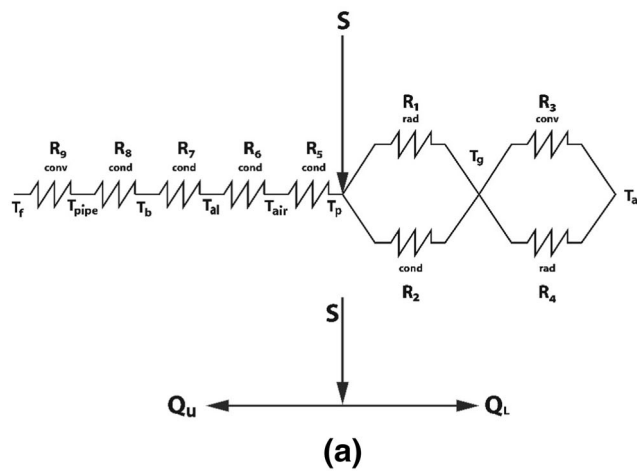

Fig. 1 Thermal network and physical model of an evacuated tube

according to the thermal network, the thermal loss can be expressed as follows:

$$Q_u = S - Q_L \tag{1}$$

$$Q_L = U_L(T_p - T_a) \tag{2}$$

$$Q_u = A_c[I_T(\tau\alpha)_e - U_L(T_p - T_a)] \tag{3}$$

S is the amount of solar energy collected by absorber tube. Q_u is the net useful energy absorbed and transferred the working fluid by the absorber tube after the heat losses to the surrounding and I_T is the total solar radiation from the sun. A_c is the outer surface area of the absorber tubes. $(\tau\alpha)$ is transmittance-absorptance product that is also called optical efficiency of the solar collector. The overall heat loss coefficient of the solar collector is as follows:

$$U_L = U_t + U_e \tag{4}$$

where U_e is the loss coefficient of the header tube edge. It is a variable term that depending on the thickness of insulation, thermal conductivity and surface areas of the header tube. The value of edge loss is 0.1687 W/(m² K) from experimental results [30]. U_t is the heat loss coefficient from the selective coating (absorber) to the surrounding and it can be expressed as:

$$U_t = \frac{1}{\dfrac{1}{h_{g-a}} + \dfrac{1}{h_{p-g}}} \tag{5}$$

where h_{g-a} is the heat transfer coefficient due to the convection from the outer glass tube to the ambient. This value was found as 12.7 W/(m² K) [30] and also the amount of heat transfer due to radiation from outer glass tube to the ambient was neglected in this case because of very small magnitude.

$$h_{p-g} = h_{p-g,r} + h_{p-g,c} \tag{6}$$

h_{p-g} is the summation of coefficient of radiation and conduction heat transfer between the absorber tube and the glass tube. $h_{p-g,c}$ is given as 0.2796 W/(m² K) [30]. Also $h_{p-g,r}$ is the function of T_p (absorber tube temperature) and T_g (outer glass tube temperature):

$$h_{p-g,r} = \frac{\sigma\varepsilon_p}{1 + \dfrac{\varepsilon_p D}{\varepsilon_g D_g}(1-\varepsilon_p)}\left(T_p^2 + T_g^2\right)\left(T_p + T_g\right) \tag{7}$$

where ε_p is selective coating emissivity, ε_g is the glass tube emissivity. D is the outer diameter of the absorber tube, D_g is the outer glass diameter and σ is the Stefan-Boltzman constant ($\sigma = 5.67 \times 10^{-8}$). The balance equation of heat loss of the evacuated tube can be expressed from the Fig. 3.

$$U_t(T_p - T_a) = h_{p-g,r}(T_p - T_g) + h_{p-g,c}(T_p - T_g) \tag{8}$$

The parameters of the absorber temperature (T_p) and the ambient temperature (T_a) are given the unknown parameters in eqs. (4-8). In this case, the bond temperature (T_b) and the working fluid outlet temperature (T_o) were obtained from the results of the calculations. The bond temperature is equal to the wall temperature of the U-tube. Unknown parameters are obtained by using different ambient temperatures with CFD results. Consequently, the overall loss coefficient can be calculated. Also, technical data of EUSC for calculations are given in Table 1.

In order to simplify the energy analysis of fin, it was assumed that the absorber tube was parallel to the aluminum fin, therefore it can be taken as a flat plate. The temperature of the absorber tube is assumed to be constant and radial temperature gradient for fin is neglected [31]. The collected energy is absorbed by selective coating and it is transferred to working fluid via aluminum fin and the U-tube respectively. Thus, variable temperature distribution is occurred over the aluminum fin for peripheral direction. The absorber tube temperature is assumed to be constant as flat plate collector. Figure 2 is given to show the energy balance for the flow domain on the aluminum fin by using elemental analysis. The U-tube diameter is d, the thickness of the aluminum fin is t, and the circumferential distance between U-tubes is W.

Energy balance equation for an elemental area of width Δx and unit length in the flow domain can be expressed as [32]:

$$-kt\frac{dT}{dx}\Big|_x - \left(-kt\frac{dT}{dx}\Big|_{x+\Delta x}\right) + Q_u\Delta x = 0 \qquad (9)$$

where k is the conductivity of aluminum fin, Q_u is the useful heat transferred to the working fluid of solar collector and t is the thickness of the aluminum fin. Q_u is also can

Table 1 Technical data of EUSC

Parameter	Value
Outer tube diameter	47 mm
Inner tube diameter (absorber)	38 mm
Thickness of the glass	1 mm
Outer diameter of U-tube	10 mm
Thickness of U-tube	0.50 mm
Solar collector length	1800 mm
Transmittance (τ)	0.91
Absorptivity of the absorber tube (α)	0.93
Absorber tube emissivity	0.06
Aluminum fin thickness	0.25 mm
Thermal conductivity of aluminum fin	202 W/m K
Thickness of air gap	1.5 mm
Thermal conductivity of air gap	0.0267 W/mK
Bond Conductance	30 W/mK
Synthetic Conductance	29 W/mK

be defined energy balance between the absorber tube and aluminum fin as:

$$Q_u = \frac{T_p - T}{\frac{t_p}{k_a} + \frac{t_{air}}{k_{air}}} = C_s(T_p - T) \qquad (10)$$

t_c and t_{air} are thickness of the absorber tube and the air gap, respectively. k_a and k_{air} are corresponding thermal conductivities. C_s is a synthetical conductance. The absorber tube temperature can be written as:

$$T_p = \frac{S + U_L T_a + C_s T}{U_L + C_s} \qquad (11)$$

If Eqs. (10) and (11) are written into Eq. (9), the energy equation of the elemental area of the fin can be yielded:

$$\frac{d^2 T}{dx^2} = \frac{S + U_L(T_a - T)}{kt\left(1 + \frac{U_L}{C_s}\right)} \qquad (12)$$

where T_a is ambient temperature. In order to solve the equation, two boundary conditions are necessary [32]:

$$\frac{dT}{dx}\Big|_{x=0} = 0 \quad \text{and} \quad T|_{x=\frac{W-d}{2}} = T_b \qquad (13)$$

Then, the solution of the differential equation can be determined as follows:

$$T = \frac{\cos mx}{\cos\left(\frac{m(W-d)}{2}\right)}\left(T_b - T_a - \frac{S}{U_L}\right) + T_a + \frac{S}{U_L} \qquad (14)$$

where m:

$$m = \sqrt{\frac{U_L}{kt\left(1 + \frac{U_L}{C_s}\right)}} \qquad (15)$$

Equation (14) denotes distribution of temperature in the x-direction of the aluminum fin. The net heat gain is equal to sum of energy collected from U-tube via aluminum fin and absorber tube. This value is also equal to the amount of energy transferred to the fluid. Heat transfer equations of fin base can be written as:

$$q_{fin} = \frac{(W-d)[S - U_L(T_b - T_a)]F}{2\left(1 + \frac{U_L}{C_s}\right)} \qquad (16)$$

Equation (16) indicates that the energy collection of one side of the U-tube and it can be rewritten for both sides:

$$q_{fin} = \frac{(W-d)[S - U_L(T_b - T_a)]F}{1 + \frac{U_L}{C_s}} \qquad (17)$$

Fig. 2 Energy balance on aluminum fin
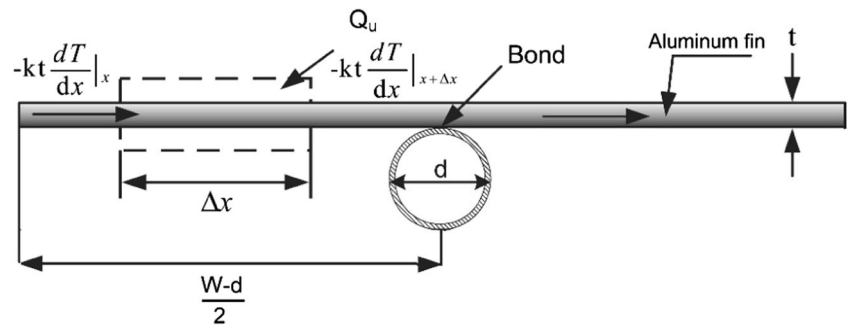
Also, the energy collection of copper U-tube can be expressed as;

$$q_{tube} = \frac{d\left[S - U_L\left(T_b - T_a\right)\right]}{1 + \dfrac{U_L}{C_s}} \tag{18}$$

Then, the net heat gain equation can be written as:

$$q_u = q_{fin} + q_{tube} = \frac{\left[(W-d)F + d\right]\left[S - U_L\left(T_b - T_a\right)\right]}{1 + \dfrac{U_L}{C_s}} \tag{19}$$

The term F is the standard fin efficiency for straight fins with rectangular profile.

$$F = \frac{\tanh\left(\dfrac{m(W-d)}{2}\right)}{\dfrac{m(W-d)}{2}} \tag{20}$$

Transferred net useful energy to the fluid:

$$q_u = \frac{T_b - T_{fl}}{\dfrac{1}{h_f \pi d} + \dfrac{1}{C_b}} \tag{21}$$

where h_f is the heat transfer coefficient between fluid and the tube wall. C_b represents the bond conductance and the value is less than 30 W/(m K) [32]. T_f is working fluid mean temperature. Solving Eq. (21) for T_b and substituting the result into the Eq. (19) the net heat gain is obtained as:

$$q_u = WF'\left(S - U_L\left(T_{fl} - T_a\right)\right) \tag{22}$$

The collector efficiency factor (F') and the h_f term can be expressed as:

$$F' = \frac{\dfrac{1}{U_L}}{W\left(\dfrac{1 + \dfrac{U_L}{C_s}}{U_L((W-d)F + d)} + \dfrac{1}{h_f \pi d} + \dfrac{1}{C_b}\right)} \tag{23}$$

$$h_f = \frac{1}{\dfrac{1}{h_{nf}} + \dfrac{t_t}{k_t}} \tag{24}$$

The net heat transferred to the working fluid in the copper U-tube can be calculated using the following expression:

$$Q_{fl} = \dot{m}c_p(T_o - T_i) \tag{25}$$

$$\dot{m} = \rho_{nf}\dot{V} \tag{26}$$

The thermal efficiency of a solar collector is defined as:

$$\eta = \frac{\dot{m}c_p(T_o - T_i)}{I_T A_p} \tag{27}$$

where A_p is the aperture area of the evacuated tube solar collector. The thermal efficiency can also be expressed as follows:

$$\eta = F_R(\tau\alpha) - F_R U_L \frac{(T_i - T_a)}{I_T} \tag{28}$$

where F_R is the heat removal factor of the solar collector and $(T_i - T_a)/I_T$ is the heat loss parameter and also called as reduced temperature.

3 Properties of nanofluid

Nanofluids consist of mixture of solid metallic or nonmetallic nanoparticles and base fluid such as water, oil, ethylene glycol etc. They have improved thermal properties compared with their base fluids. Significant improvement can be obtained in convective heat transfer for energy applications using nanofluids as working fluids. There has been various types and numbers of studies about nanofluids and its applications after Choi et al. [33] proposed using nanofluids.

Nanofluids are assumed to be homogeneous and stable in this study. Different types of nanofluids (ZnO/EG-PW, Ag/EG-PW and MgO/EG-PW) were used at different concentrations (1.0%, 2.0%, 3.0 and 4.0%) in a EUSC. The thermophysical properties of each nanoparticle and base fluid are given in Table 2.

Table 2 Thermophysical properties of nanoparticle and base fluid [34]

Material	Density (kg/m³)	Thermal conductivity (W/m K)	Specific heat (j/kg K)
ZnO	5630	21	494
Ag	10,500	426.7	236
MgO	3580	42	877
EG-PW	1032.1	0.506	3650.5

In order to calculate the heat transfer coefficient for nanofluid, choosing thermophysical models for nanofluid has vital importance. These mentioned necessary thermophysical properties are density, viscosity, specific heat and thermal conductivity. The subscripts for referring to elements of nanoparticles, the base fluid and the nanofluid in the following equations are "np"," f" and" nf", respectively.

The density and the specific heat of the nanofluids were obtained using the equations below [35]:

$$\rho_{nf} = \left(\frac{\phi}{100}\right)\rho_p + \left(1 - \frac{\phi}{100}\right)\rho_f \tag{29}$$

$$C_{nf} = \frac{\frac{\phi}{100}(\rho C)_p + \left(1 - \frac{\phi}{100}\right)(\rho C)_f}{\rho_{nf}} \tag{30}$$

where φ is volumetric concentration of the nanoparticle.

The correlations below were used to obtain the thermal conductivity and viscosity [36].

$$k_{nf} = k_{bf}\frac{k_{np} + 2k_{bf} + 2\phi(k_{np} - k_{bf})}{k_{np} + 2k_{bf} - \phi(k_{np} - k_{bf})} \tag{36}$$

$$\mu_{nf} = \frac{\mu_{bf}}{(1-\phi)^{2.5}} \tag{37}$$

It is assumed that the tube is under constant heat flux and also the flow is laminar as mentioned before. Shah [37] equations can be used for calculating the Nusselt number which is valid for these conditions. The Reynolds number, average Nusselt number and the average convective heat transfer co-efficient of the nanofluids can be expressed as:

$$\text{Re} = \frac{4\dot{m}}{\pi d\mu_{nf}} \tag{32}$$

$$Nu = \begin{cases} 1.953\left(\text{RePr}\frac{d}{x}\right)^{1/3} & : \left(\text{RePr}\frac{d}{x}\right) \geq 33.33 \\ 4.634 + 0.0722\left(\text{RePr}\frac{d}{x}\right) & : \left(\text{RePr}\frac{d}{x}\right) < 33.33 \end{cases} \tag{33}$$

$$h_{nf} = \frac{Nuk_{nf}}{d} \tag{34}$$

Enhancement of nanoparticle concentration provides higher thermal conductivity until the optimum level.

Because at higher concentrations viscosity reach up to undesirable values so this causes higher pumping power. Aggregation and sedimentation occur higher than optimum values of concentration. These circumstances can cause instability of nanofluids. In previous studies it has been reported that the thermal performance of nanofluids was significantly improved at under certain volumetric concentrations which was 5.0% [38–40].

According to previous studies the nanoparticle volume concentrations were set at 1.0% – 4.0% and calculations was made between these values. Thermal performance of a EUSC was evaluated by using ZnO, Ag and MgO nanoparticles in antifreeze base fluid (30:70; EG:PW) as collector working fluids under various operating conditions.

4 Solution procedure

In this study, in order to perform the numerical analysis, a general finite – volume based commercial CFD software ANSYS FLUENT 17.0 was used. Computations were conducted under laminar flow condition (Re < 2300). The continuity, Navier – Stokes and energy equations were solved numerically until the residuals lower than 10^{-6} through the iterative process. In numerical analysis, the copper U-tube was modelled with the same dimensions as a real solar collector. The length and the diameter of the U-tube are L = 4 m and d = 0.009 m. Illustration of structure of an EUSC given in Fig. 3.

The thermophysical properties of nanofluids were obtained at the mean temperature in the copper U-tube. The continuity, momentum and energy equations were solved iteratively and given in below in cylindrical coordinates [41].
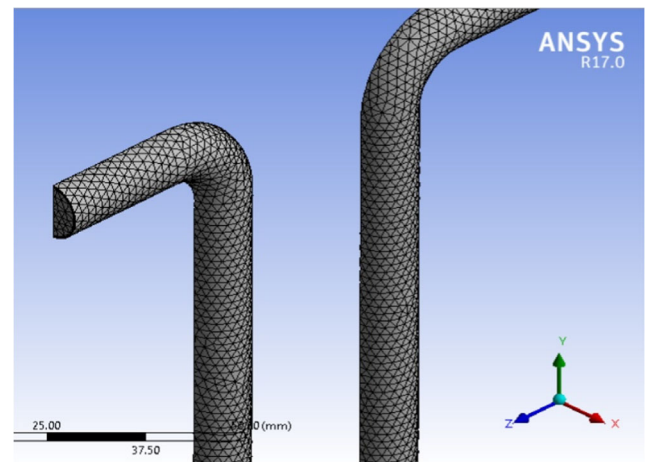
Continuity equation:

$$\nabla\vec{V}^* = 0 \tag{35}$$

Fig. 3 Illustration of structure of an EUSC

Momentum equation:

$$\left(\overrightarrow{V}^{*}\nabla^{*}\right)\overrightarrow{V}^{*} = -Eu\nabla^{*}P^{*} + \mathrm{Re}\nabla^{*2}\overrightarrow{V}^{*} \quad (36)$$

Energy equation:

$$\frac{1}{\mathrm{RePr}}\nabla^{*2}T^{*} + \frac{E_c}{\mathrm{Re}}\Phi^{*} = 0 \quad (37)$$

where the dimensionless parameters in the Eqns. (35)–(37):

$$\overrightarrow{V}^{*} = \frac{\overrightarrow{V}}{U_m}, \quad \overrightarrow{\nabla}^{*} = \overrightarrow{\nabla}D_h, \quad \mathrm{Re} = \frac{\rho V D_h}{\mu}, \quad P^{*} = \frac{P - P_\infty}{P_0 - P_\infty}, \quad g^{*} = \frac{\overrightarrow{g}}{g},$$

$$T^{*} = \frac{T - T_\infty}{T_w - T_\infty}, \quad \mathrm{Pr} = \frac{\mu c_p}{k}, \quad Ec = \frac{U_m^2}{c_p(T_0 - T_m)}, \quad Eu = \frac{P_0 - P_\infty}{\rho V^2}$$

Uniform velocity (mass flow rate) and temperature profile of each nanofluid was performed at the inlet of the U-tube. The no slip boundary condition and uniform surface heat flux were applied on the U-tube walls. The pressure outlet boundary condition was performed at the outlet of the U-tube. Also, the symmetry boundary condition was used on the symmetry plane.

Tetrahedron cells were generated with a fine mesh near the tube walls. To obtain the fine mesh distribution, boundary layer mesh type was used at the adjacent to the surfaces of the pipe. As depicted a part of U-tube in Fig. 4, the non – uniform grid distribution was performed to the plane perpendicular to the main flow direction. In order to enhance the resolution and accuracy, the amount of mesh was enhanced close to each wall.

In order to discretization of convection terms, second order upwind scheme was used. The standard scheme was employed for discretization of the pressure and SIMPLE algorithm was used to resolve the coupling between the velocity and pressure [42]. No convergence problems were observed during the calculations.
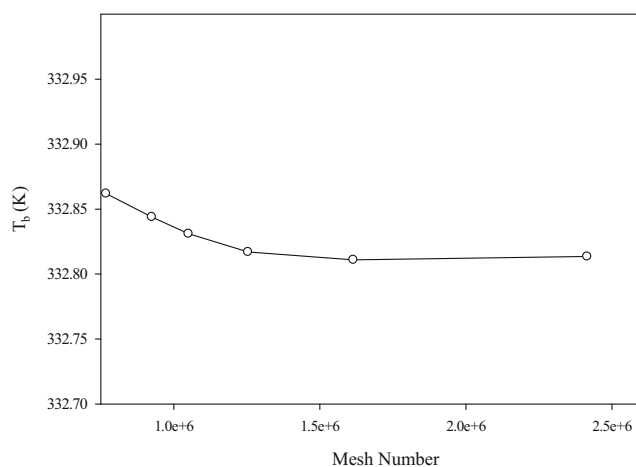
5 Results and discussion

The mesh independence study was carried out until the variation in U-tube wall temperature which is also equal to bond temperature (T_b) was less than 1.0%. To provide the certainty of results, a grid independence study was performed for pure water flow using eight different grid sizes changing from 7.67×10^5 to 2.48×10^6 for constant mass flow rate. This process gave the effects of grid size on the solution. It is illustrated in Fig. 5 that there was no remarkable variation on U-tube wall temperature between 1.6×10^6 and 2.4×10^6 grid sizes. According the mesh independence process, the grid size 1.6×10^6 was chosen for optimum grid size for this study.

This study investigates the accuracy of the theoretical results for thermal performance of a EUSC by using different types of nanofluids. In order to test the accuracy of the numerical approach, the efficiency profiles of the EUSC compared with the experimental results of Yin et al. [25] in Fig. 6 for pure water as working fluid. Thermal efficiency curve of EUSC is created as a function of reduced temperature ($T_i - T_a$)/I_T. The heat loss parameter is the significant parameter for determining the instant efficiency of the solar collector. It is observed that the current results of thermal efficiency are harmonious with the experimental results. The average deviation between results of this study and experimental ones is about 3.1%.

Figure 7 represents the variation of overall heat loss coefficient and the radiation heat loss coefficient from the absorber tube to the ambient as a function of ($T_p - T_a$) for EG-PW as a working fluid. The thermal performance of a solar collector is affected by overall loss coefficient very significantly. This value increases with increasing the temperature of ambient and also with ($T_p - T_a$). The overall heat loss coefficient from the absorber tube to the ambient is maximum at the maximum temperature difference of ($T_p - T_a$) as the value of 1.21 W/m^2 K at the 313 K ambient temperature. The behavior of
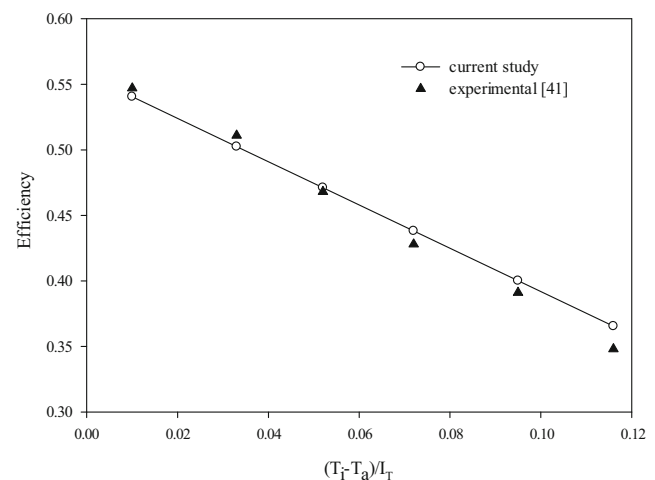

Fig. 4 Mesh distribution of computational domain

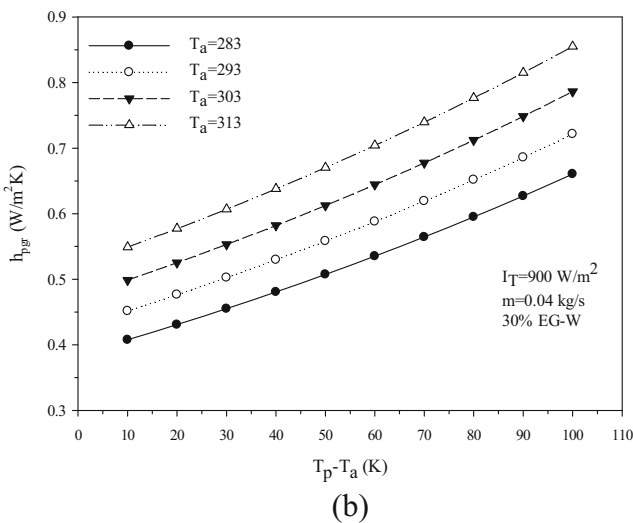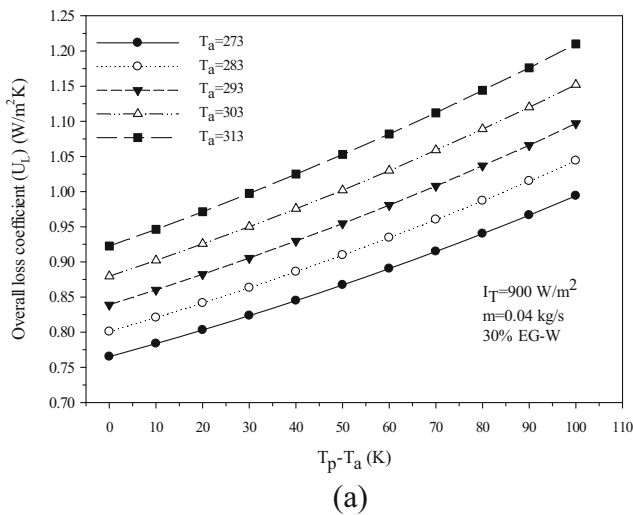**Fig. 5** Variation of bond temperature (T_b) with mesh number

(a)

(b)

Fig. 6 Comparison of current study with experimental results in the literature
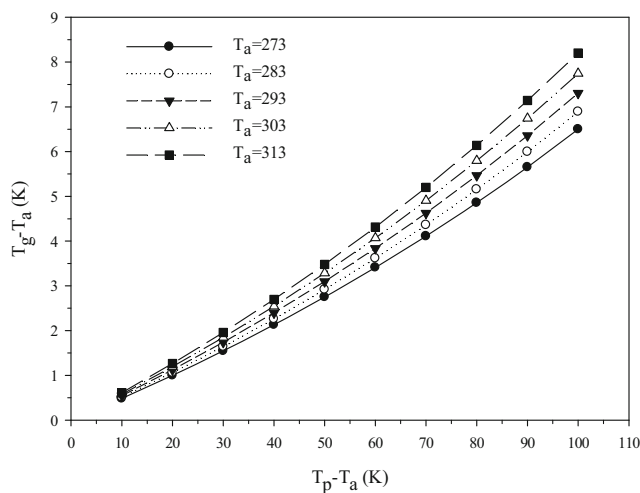

Fig. 7 Variation of overall heat loss coefficient (a) and radiation heat loss coefficient (b) from the absorber tube to the outer glass tube as a function of $(T_p\text{-}T_a)$ for different ambient temperatures

enhancement overall loss coefficient is gradually increasing as indicated in Kim et al. [43]. The radiation heat loss coefficient value (h_{pgr}) depend on the temperatures of ambient and absorber tube as indicated in Eq. (7). It is clearly obtained from the Fig. 7b, the radiation heat loss coefficient from absorber tube to the ambient increases with increasing of $(T_p\text{-}T_a)$ at the same ambient temperature. The radiation heat transfer coefficient is greater than the conduction heat transfer coefficient (h_{pgc}) prominently that the (h_{pgr}) value reaches to 0.86 W/m^2 K at the 313 K ambient temperature and 100 K temperature difference $(T_p\text{-}T_a)$.

The variation of temperature difference $(T_g\text{-}T_a)$ according to the value of $(T_p\text{-}T_a)$ at different ambient temperatures for EG-PW as working fluid is given in Fig. 8. The temperature difference $(T_g\text{-}T_a)$ increases nonlinearly with increasing of $(T_p\text{-}T_a)$. The magnitude of $(T_g\text{-}T_a)$ reaches the highest value at the higher ambient temperature and $(T_p\text{-}T_a)$ value. This means the thermal loss increases when the ambient temperature increases. The temperature distribution on the fin according to its length is given in Fig. 9 with 283 K inlet temperature. The maximum value of the fin temperature takes place at the intersection of the fin and the U-tube and it is also equal to the bond temperature (T_b).

The changing of collector efficiency factor and absorber temperature according to the $(T_f\text{-}T_a)$ for $I_T = 900$ W/m^2, $T_a = 283$ K, $C_s = 29$ W/m K given in Fig. 10. The collector efficiency factor decreases slightly with increasing the $(T_f\text{-}T_a)$. Furthermore, the absorber temperature increases from 325 K to 455 K linearly with increasing the $(T_f\text{-}T_a)$.

The variation of temperature difference between the inlet and outlet of the solar collector for different types of nanofluids and the mass flow rates according to the inlet temperature is given in Fig. 11. As the inlet temperature of working fluid increases, the heat loss from the solar collector increases. Also, the decrease in temperature difference between the inlet and outlet causes decreasing in net heat gain of the working fluid. It is clearly seen from the Fig. 11 that the
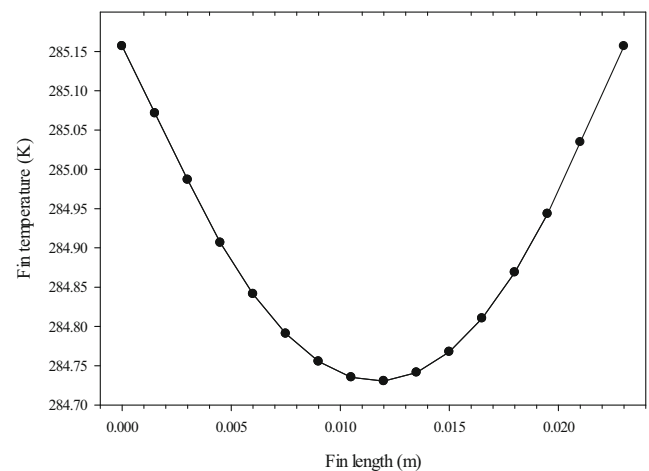

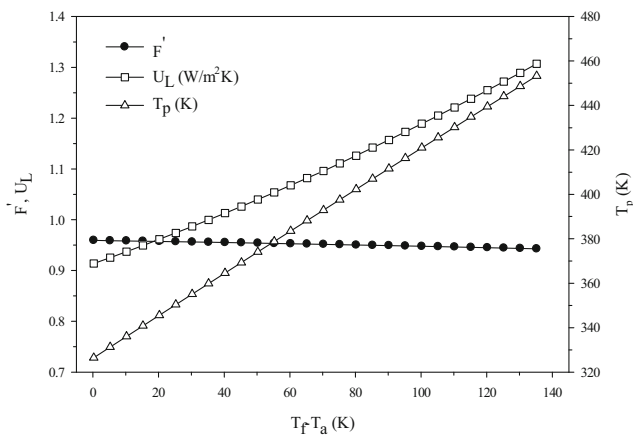**Fig. 8** Variation of $(T_g\text{-}T_a)$ with $(T_p\text{-}T_a)$

Fig. 9 Temperature distribution of the fin for EG-PW working fluid and $T_i = 283$ K

temperature difference decreases with the increasing the inlet temperature. The outlet temperature of the EUSC decreases about 0.5 K when the inlet temperature increases from 303 to 353 K at the value of the mass flow rate is 0.001 kg/s, while the decrease is 0.14 K at 0.003 kg/s under the same condition. The 4.0 vol.% Ag/EG-PW nanofluid has the greatest outlet temperature of the collector at each mass flow rate. These values are greater than Ma's results that the values of them are 0.65 K for 0.003 kg/s and 1.96 K for 0.001 kg/s since the working fluid of them was water. Nanofluids collects more energy than pure water and thus the temperature difference is higher than pure water and the reduction of temperature difference is smaller than water.

Figure 12 represents the variation of the collector efficiency factor for different overall loss coefficients as a function of the synthetical conductance, C_s. The collector efficiency factor, F', increases rapidly until the synthetical conductance is about 40 W/m.K, and then it reaches at the constant value as reported before by Ma et al. [44]. The results of them are slightly greater than this study since the working fluid is water in their
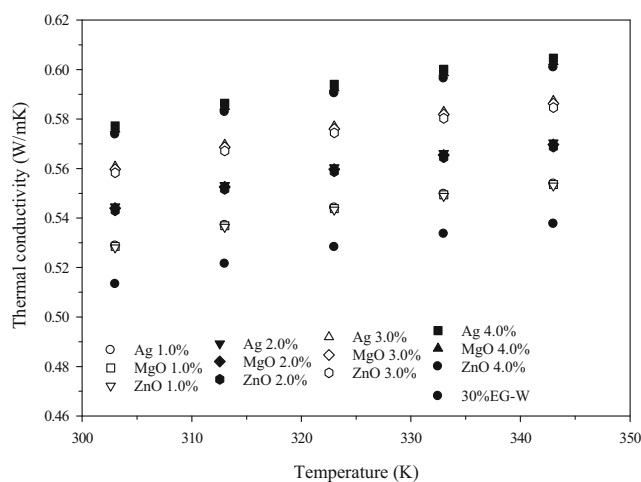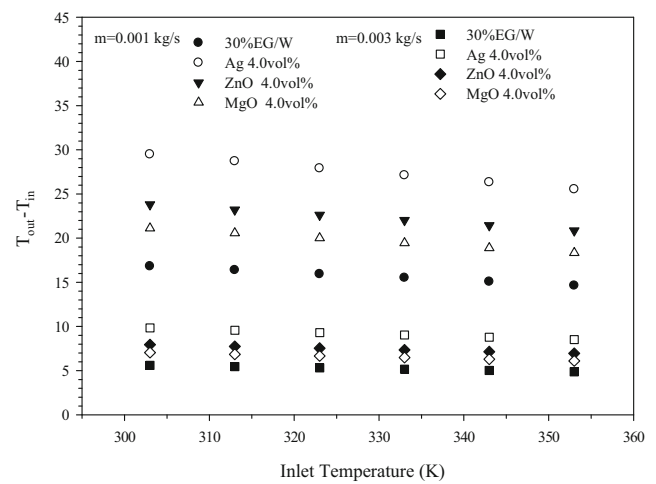

Fig. 11 Variation of the temperature difference between the outlet and inlet temperature

study. This shows that the effect of thermal resistance of air layer on collector efficiency is very significant. This enhancement of C_s causes the reduction of collector efficiency.

Figure 13 shows the variation of the collector efficiency according to the solar radiation for different types of nanofluids. The efficiency of collector has upward tendency with solar irradiance when the temperature difference between inlet and ambient is constant. This enhancement trend continues gradually until the rate is constant. It is obtained that using nanofluid in a solar collector provides higher collector efficiency than using the base fluid at the same condition. When using the Ag/EG-PW nanofluid at the volume concentration of 4.0% as the working fluid according to base fluid of EG-PW, the improvements in the collector efficiency is 22.7 and 25.8% for the solar radiation is at 200 W/m^2 and 1000 W/m^2, respectively. The collector efficiency increases with increasing the solar radiation. The lowest value of the collector efficiency is obtained for ZnO/EG-PW nanofluid at the nanoparticle concentration of 4.0 vol% with the efficiency increment is 12.6 and 13.4% for
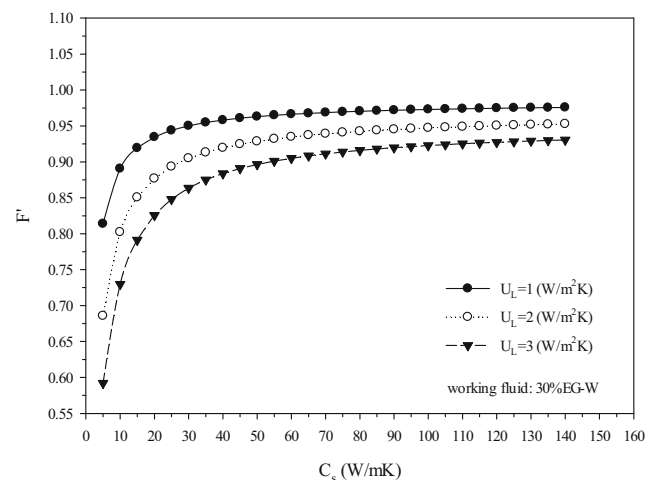

Fig. 10 Variation of the F', U_L and T_p according to difference of working fluid mean temperature and ambient temperature

Fig. 12 Collector efficiency factor vs. synthetical conductance
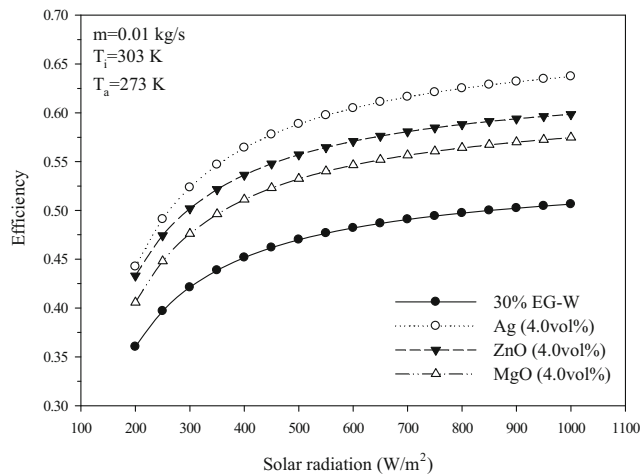
Fig. 13 Variation of the solar collector efficiency with solar radiation for different types of nanofluids

the solar radiation is at 200 W/m² and 1000 W/m², respectively, at the same operating condition. The solar collector efficiency is growing rapidly until the solar radiation is about 300 W/m² as reported by Kim et al. [43]. The enhancement of the collector efficiency reaches nearly at the constant value after the solar radiation is 800 W/m² due to the limitation of heat transfer capability of solar collector.

Variation of the solar collector efficiency with the heat loss parameter $((T_i-T_a)/I_T)$ for different types of nanofluids is given in Fig. 14. It can be seen that the collector efficiency is generally directly proportional to the types of nanofluids. The highest collector efficiency is obtained when the working fluid inlet temperature is equal to the ambient temperature as shown in Fig. 14 for all types of nanofluids. In other words, the collector efficiency is inversely proportional to the $((T_i-T_a)/I_T)$. The collector efficiency values are at 68.7 and 46.1% for Ag/EG-PW nanofluid when $(T_i-T_a)/I_T$ values are equal to 0 and 0.14, respectively. Also, these values are higher than the base fluid about at 26.4 and 24.8% at the same condition. In addition,
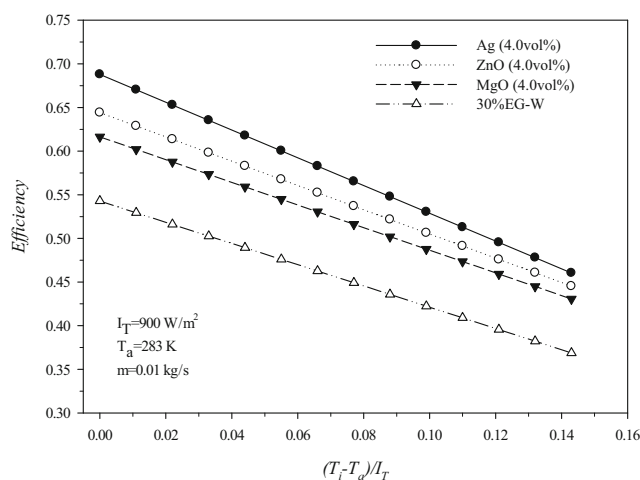
using ZnO/EG-PW nanofluid in the volume concentration of 4.0% provides the 13.5 and 13.3% improvements in collector efficiency according to using base fluid, when $((T_i-T_a)/I_T)$ values are equal to 0 and 0.14, respectively. The efficiency improvement for using MgO/EG-PW nanofluid as working fluid is 5.26%. According to the experimental results of Verma et al. [45], the efficiency enhancement of using MgO/PW nanofluid in a flat plate solar collector is about 4.8%.

Figure 15 represents the variation of collector efficiency according to nanoparticle volume concentration for different types of nanofluids. It is seen from the figure that the collector efficiency increases with increasing the nanoparticle volume concentration of the nanofluid. In addition, the Ag/EG-PW nanofluid with the 4.0% nanoparticle volume concentration can be determined as the most effective choice to use as a working fluid in an EUSC. The heat transfer capability of Ag nanoparticle is better than the other nanoparticles since it has the lowest specific heat and highest thermal conductivity and density. The collector efficiency for using ZnO/EG-PW nanofluid as working fluid is greater than the collector

(a) $(T_i-T_a)/I_T=0$.
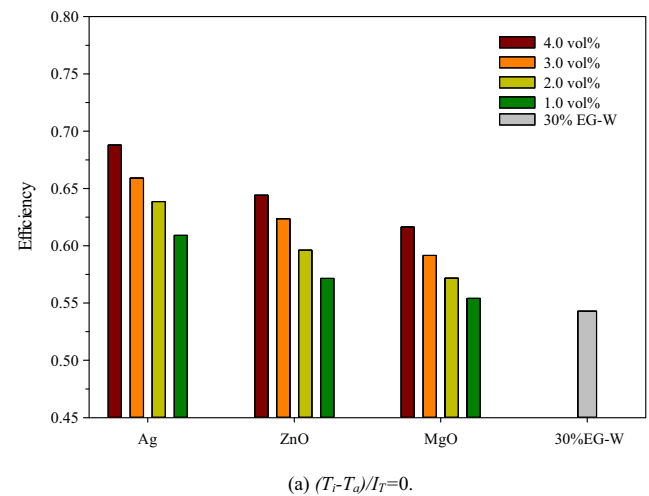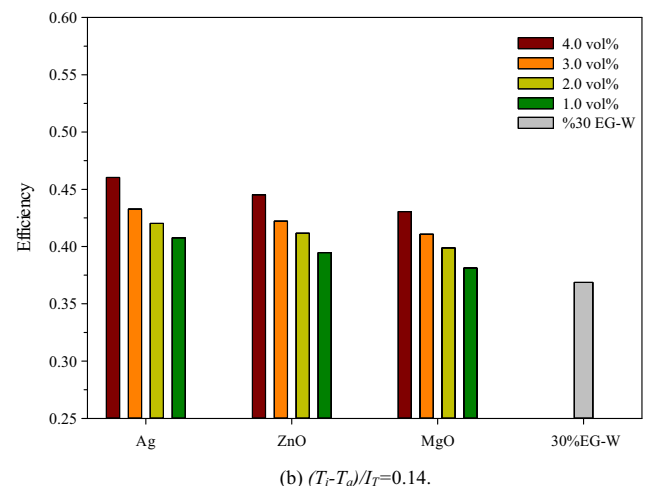
(b) $(T_i-T_a)/I_T=0.14$.

Fig. 15 Variation of the collector efficiency for different volume concentrations of nanofluids

Fig. 14 Variation of the collector efficiency with $(T_i-T_a)/I_T$ for different types of nanofluids

Table 3 Variation of monthly average solar radiation and ambient temperature in Karabük, Turkey

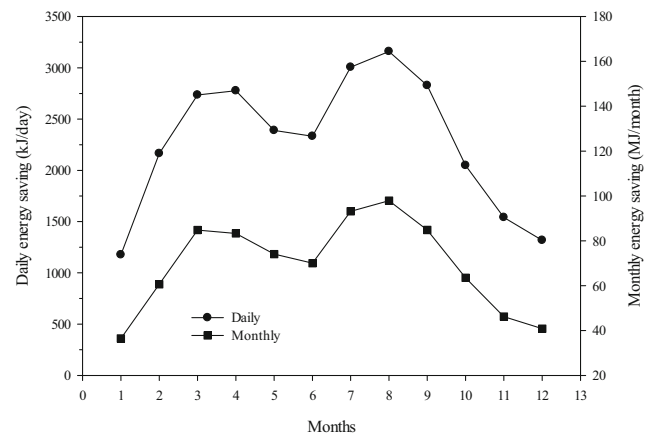| Month	Solar radiation (MJ/m²/month)	Ambient temperature (°C)
1	255.6	2.9
2	434.4	4.8
3	533.8	8.0
4	532.9	12.8
5	453.5	17.4
6	436.8	21.0
7	555.3	24.0
8	584.1	23.7
9	530.6	19.5
10	396.3	14.2
11	313.4	8.2
12	279.4	4.2

Fig. 16 Variation of the daily and monthly energy saving with months

efficiency for using MgO/EG-PW nanofluid at the same condition. Although, ZnO nanoparticle has lower thermal conductivity than MgO nanoparticle, the heat transfer performance of ZnO nanoparticle is greater than MgO nanoparticle using in an EUSC, as also reported by Li et al. [46].

Table 3 shows the monthly average solar radiation and ambient temperatures in Karabük, Turkey having terrestrial coordinates of 41 °N and 32 °E [47]. It can be seen from the Table 3 that the measured data for solar radiation in August is the maximum value for all over the year while having lowest value in January. Also, the reduction of coal usage and harmful gases (CO_2 and SO_2) generation are given in Table 4 for installed 30 units of EUSC with using different types of nanofluids as working fluid. It is obtained that using EUSC instead of using coal for heating process helps the reduction of generation of the harmful gases and coal usage. The amount of generation of total energy is 29,306 kJ when 1 kg coal is fully combusted [48]. The largest coal usage reduction is 855.5 kg/year for 4.0 vol.% Ag/EG-PW nanofluid since the highest collector efficiency is achieved for Ag/EG-PW nanofluid. The corresponding CO_2 and SO_2 reduction for 4.0 vol.% Ag/EG-PW nanofluid is 2241.4 kg and 7.2 kg per year, respectively. Using the EUSC with nanofluids as working fluid instead of base fluid provides as the range of 91.9 – 176.7 kg

for coal reduction, 240.7 – 462.7 kg for reduction of CO_2 generation and 0.8 – 1.5 kg for reduction of SO_2 generation.

The daily and monthly energy saving for using 4.0 vol% Ag/EG-PW nanofluid as a working fluid in EUSC is shown in Fig. 16. It can be seen from the figure that the highest monthly energy saving occurs in August as the rate of 97.9 MJ, while the lowest value is 36.4 MJ in January.

Figure 17 represents the variation of reduction of consumption and cost of electricity of different countries according to number of solar collector for using 4.0 vol.% Ag/EG-PW nanofluid in the EUSC under operating conditions in Table 4. The energy saving of using single collector with 4.0 vol.% Ag/EG-PW nanofluid is 172.5 MJ higher than using the base fluid per year. Thus, the yearly saving for 30 solar collectors is found as 5176 MJ higher than using the base fluid. The yearly total energy saving when installing 30 collectors is 25,071 MJ for 4.0 vol.% Ag/EG-PW nanofluid as a working fluid and the amount of corresponding electricity reduction is 6964.1 kWh for this condition. One of the highest electricity unit price around the world is in Denmark ($0.35/kWh). Thus, installing the 30 collectors array saves $2486.1 per year in Denmark. Furthermore, the amount of cost savings

Table 4 Reduction of coal usage and harmful gases generation for different types of nanofluids using in EUSC

Type of Nanofluid	Coal weight (kg)	CO₂ weight (kg)	SO₂ weight (kg)
4.0 vol.% Ag/EG-PW	855.5	2241.4	7.2
4.0 vol.% ZnO/EG-PW	801.5	2100.1	6.8
4.0 vol.% MgO/EG-PW	770.7	2019.4	6.5
EG-PW	678.8	1778.7	5.7
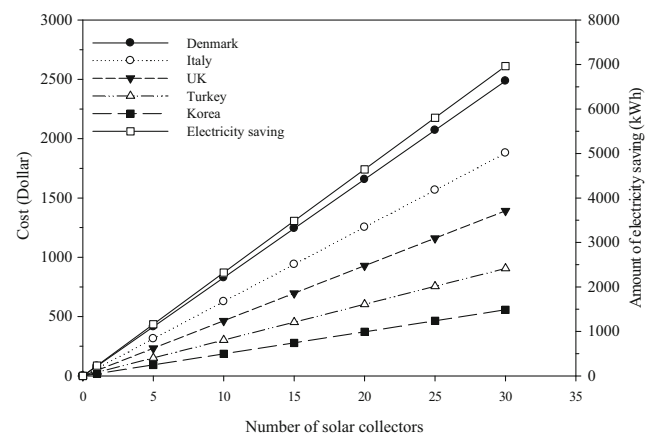
Fig. 17 Variation of cost of electricity and the amount of energy saving as a function of number of solar collectors for different countries

under the same conditions in Italy, UK, Turkey and South Korea are \$1880.3, \$1392.8, \$905.3 and \$557.1, respectively [49, 50]. This study reveals that using nanofluids in EUSC as working fluids has notable effect in energy saving and reduction of CO_2 and SO_2.

6 Conclusion

Numerical analysis for performance of an evacuated U-tube solar collector using nanofluids was conducted in this study. An antifreeze solution EG-PW was used as base fluid. It is found that the thermal conductivity is proportional with the temperature and volume concentration. The maximum collector efficiency is achieved for Ag/EG-PW nanofluid as a working fluid in EUSC at the 4.0% volume concentration. The average efficiency enhancement for nanoparticle addition into the base fluid is about 8.0% for the changing of volume concentration from 1.0 to 4.0%.

The reductions of coal usage and harmful gases (CO_2 and SO_2) generation increases with using nanofluid in EUSC as a working fluid, when 30 collectors are installed in Karabük having the coordinates at 41 $^{\mathrm{o}}$N and 32 $^{\circ}$E. It is also obtained that, using 4.0 vol.% Ag/EG-PW nanofluid in EUSC causes the maximum reduction of coal usage and CO_2 and SO_2 generation. Furthermore, a remarkable efficiency improvement using 4.0 vol.% Ag/EG-PW nanofluid provides 6964.1 kWh electricity saving per year which is 1437.7 kWh higher than that of using base fluid. The maximum cost saving can be achieved as \$2486.1 when the collectors are installed in Denmark.

Compliance with ethical standards

Conflict of interest On behalf of all authors, the corresponding author states that there is no conflict of interest.

Publisher's Note Springer Nature remains neutral with regard to jurisdictional claims in published maps and institutional affiliations.

References

1. Thirugnanasambandam M, Iniyan S, Goic R (2010) A review of solar thermal technologies. Renew Sust Energ Rev 14:312–322. https://doi.org/10.1016/j.rser.2009.07.014
2. Gao Y, Fan R, Zhang XY, An YJ, Wang MX, Gao YK, Yu Y (2014) Thermal performance and parameter analysis of a U-pipe evacuated solar tube collector. Sol Energy 107:714–727. https://doi.org/10.1016/j.solener.2014.05.023
3. Kim Y, Seo T (2007) Thermal performances comparisons of the glass evacuated tube solar collectors with shapes of absorber tube. Renew Energy 32:772–795. https://doi.org/10.1016/j.renene.2006.03.016
4. Li Y, Fernández-Seara J, Du K, Pardiñas ÁÁ, Latas LL, Jiang W (2016) Experimental investigation on heat transfer and pressure drop of ZnO/ethylene glycol-water nanofluids in transition flow. Appl Therm Eng 93:537–548. https://doi.org/10.1016/j.applthermaleng.2015.09.020
5. Hamid KA, Azmi WH, Mamat R, Sharma KV (2016) Experimental investigation on heat transfer performance of TiO2 nanofluids in water-ethylene glycol mixture. Int Commun Heat Mass Transf 73:16–24. https://doi.org/10.1016/j.icheatmasstransfer.2016.02.009
6. Xu J, Bandyopadhyay K, Jung D (2016) Experimental investigation on the correlation between nano-fluid characteristics and thermal properties of Al2O3 nano-particles dispersed in ethylene glycol-water mixture. Int J Heat Mass Transf 94:262–268. https://doi.org/10.1016/j.ijheatmasstransfer.2015.11.056
7. Cabaleiro D, Pastoriza-Gallego MJ, Pineiro MM, Lugo L (2013) Characterization and measurements of thermal conductivity, density and rheological properties of zinc oxide nanoparticles dispersed in (ethane-1,2-diol + water) mixture. J Chem Thermodyn 58:405–415. https://doi.org/10.1016/j.jct.2012.10.014
8. Yousefi T, Veysi F, Shojaeizadeh E, Zinadini S (2012) An experimental investigation on the effect of Al2O3-H2O nanofluid on the efficiency of flat-plate solar collectors. Renew Energy 39:293–298. https://doi.org/10.1016/j.renene.2011.08.056
9. Yousefi T, Veisy F, Shojaeizadeh E, Zinadini S (2012) An experimental investigation on the effect of MWCNT-H2O nanofluid on the efficiency of flat-plate solar collectors. Exp Thermal Fluid Sci 39:207–212. https://doi.org/10.1016/j.expthermflusci.2012.01.025
10. Said Z, Sajid MH, Alim MA, Saidur R, Rahim NA (2013) Experimental investigation of the thermophysical properties of AL2O3-nanofluid and its effect on a flat plate solar collector. Int Commun Heat Mass Transf 48:99–107. https://doi.org/10.1016/j.icheatmasstransfer.2013.09.005
11. Sokhansefat T, Kasaeian A (2012) Numerical Study of Heat Transfer Enhancement by using Al2O3 / Synthetic Oil Nanofluid in a Parabolic Trough Collector Tube, in: World Acad. Sci Eng Technol 69:1154–1159
12. Kalogirou SA (2004) Solar thermal collectors and applications. Prog Energy Combust Sci 30:231–295. https://doi.org/10.1016/j.pecs.2004.02.001
13. Colangelo G, Favale E, De Risi A, Laforgia D (2013) A new solution for reduced sedimentation flat panel solar thermal collector using nanofluids. Appl Energy 111:80–93. https://doi.org/10.1016/j.apenergy.2013.04.069
14. Moghadam AJ, Farzane-Gord M, Sajadi M, Hoseyn-Zadeh M (2014) Effects of CuO/water nanofluid on the efficiency of a flat-plate solar collector. Exp Thermal Fluid Sci 58:9–14. https://doi.org/10.1016/j.expthermflusci.2014.06.014
15. Faizal M, Saidur R, Mekhilef S (2013) Potential of size reduction of flat-plate solar collectors when applying MWCNT nanofluid. IOP Conf Ser Earth Environ Sci 16:012004. https://doi.org/10.1088/1755-1315/16/1/012004
16. Mahian O, Kianifar A, Sahin AZ, Wongwises S (2014) Performance analysis of a minichannel-based solar collector using different nanofluids. Energy Convers Manag 88:129–138. https://doi.org/10.1016/j.enconman.2014.08.021
17. Gao Y, Zhang Q, Fan R, Lin X, Yu Y (2013) Effects of thermal mass and flow rate on forced-circulation solar hot-water system: Comparison of water-in-glass and U-pipe evacuated-tube solar collectors. Sol Energy 98:290–301. https://doi.org/10.1016/j.solener.2013.10.014
18. Liang RB, Zhang JL, Zhao L, Ma LD (2015) Performance enhancement of filled-type solar collector with U-tube. J Cent South Univ 22:1124–1131. https://doi.org/10.1007/s11771-015-2624-5
19. Liang R, Ma L, Zhang J, Zhao D (2011) Theoretical and experimental investigation of the filled-type evacuated tube solar collector

with U tube. Sol Energy 85:1735–1744. https://doi.org/10.1016/j.solener.2011.04.012

20. Liang R, Ma L, Zhang J, Zhao L (2013) Performance analysis of a new-design filled-type solar collector with double U-tubes. Energy Build 57:220–226. https://doi.org/10.1016/j.enbuild.2012.11.004

21. Liang R, Zhang J, Zhao L, Ma L (2014) Research on the universal model of filled-type evacuated tube with U-tube in uniform boundary condition. Appl Therm Eng 63:362–369. https://doi.org/10.1016/j.applthermaleng.2013.11.020

22. Ma L, Zhao T, Zhang J, Zhao D (2016) Numerical study on the heat transfer characteristics of filled-type solar collector with U-tube. Appl Therm Eng 107:642–652. https://doi.org/10.1016/j.applthermaleng.2016.05.133

23. Alfaro-Ayala JA, Martínez-Rodríguez G, Picón-Núñez M, Uribe-Ramírez AR, Gallegos-Muñoz A (2015) Numerical study of a low temperature water-in-glass evacuated tube solar collector. Energy Convers Manag 94:472–481. https://doi.org/10.1016/j.enconman.2015.01.091

24. Azad E (2008) Theoretical and experimental investigation of heat pipe solar collector. Exp Thermal Fluid Sci 32:1666–1672. https://doi.org/10.1016/j.expthermflusci.2008.05.011

25. Yin ZQ, Harding GL, Collins RE (1997) The thermal performance of the coaxial evacuated glass tubular solar collector. Sol Energy 2:19–20

26. Liu ZH, Hu RL, Lu L, Zhao F, Xiao HS (2013) Thermal performance of an open thermosyphon using nanofluid for evacuated tubular high temperature air solar collector. Energy Convers Manag 73:135–143. https://doi.org/10.1016/j.enconman.2013.04.010

27. Kim H, Kim J, Cho H (2017) Experimental study on performance improvement of U-tube solar collector depending on nanoparticle size and concentration of Al2O3 nanofluid. Energy 118:1304–1312. https://doi.org/10.1016/j.energy.2016.11.009

28. Tong Y, Cho H (2015) Comparative Study on the Thermal Performance of Evacuated Solar Collectors with U-Tubes and Heat Pipes. Int J Air-Conditioning Refrig 23:1550019. https://doi.org/10.1142/S2010132515500194

29. Kim JT, Ahn HT, Han H, Kim HT, Chun W (2007) The performance simulation of all-glass vacuum tubes with coaxial fluid conduit. Int Commun Heat Mass Transf 34:587–597. https://doi.org/10.1016/j.icheatmasstransfer.2007.01.012

30. Tian Q (2006) Study on thermal efficiency and performance of U-tubular all-glass evacuated tube solar collector. Energy Eng 6:36–40

31. Tian Q (2007) Thermal performance of the U-type evacuated glass tubular solar collector. Build Energy Environ 26(3):51–54

32. Duffie J, Beckman W (2006) Solar Engineering of Thermal Processes, 4th ed. John Wiley & Sons, Hoboken. https://doi.org/10.1115/1.2930068

33. Choi SUS, Eastman JA (1995) Enhancing thermal conductivity of fluids with nanoparticles. ASME Int Mech Eng Congr Expo 66:99–105. https://doi.org/10.1115/1.1532008

34. Incropera FP, Bergman TL, Lavine AS, DeWitt DP (2011) Fundamentals of Heat and Mass Transfer, 7th ed. John Wiley & Sons, Hoboken

35. Pak BC, Cho YI (1998) Hydrodynamic and Heat Transfer Study of Dispersed Fluids With Submicron Metallic Oxide Particles. Exp Heat Transf 11:151–170. https://doi.org/10.1080/08916159808946559

36. Hussein AM, Sharma KV, Bakar RA, Kadirgama K (2013) The effect of cross sectional area of tube on friction factor and heat transfer nanofluid turbulent flow. Int Commun Heat Mass Transf 47:49–55. https://doi.org/10.1016/j.icheatmasstransfer.2013.06.007

37. Shah RK (1975) Thermal entry length solutions for the circular tube and paralel plates. In: 3rd Natl. Heat Mass Transf. Conf., pp. 11–75

38. Li CH, Peterson GP (2006) Experimental investigation of temperature and volume fraction variations on the effective thermal conductivity of nanoparticle suspensions (nanofluids). J Appl Phys 99. https://doi.org/10.1063/1.2191571

39. Verma SK, Tiwari AK (2015) Progress of nanofluid application in solar collectors: A review. Energy Convers Manag 100:324–346. https://doi.org/10.1016/j.enconman.2015.04.071

40. Masuda H, Ebata A, Teramae K, Hishinuma N (1993) Alteration of Thermal Conductivity and Viscosity of Liquid by Dispersing Ultra-Fine Particles (Dispersion of Al2O3, SiO2 and TiO2 Ultra-Fine Particles). Netsu Bussei 7:227–233. https://doi.org/10.2963/jjtp.7.227

41. Bejan A (2013) Convection Heat Transfer, 4th ed. John Wiley & Sons, Hoboken. https://doi.org/10.1002/9781118671627

42. Das SK, Choi SUS, Yu W, Pradeep T (2007) Nanofluids: Science and Technology. John Wiley & Sons, Hoboken. https://doi.org/10.1002/9780470180693

43. Kim H, Ham J, Park C, Cho H (2016) Theoretical investigation of the efficiency of a U-tube solar collector using various nanofluids. Energy 94:497–507. https://doi.org/10.1016/j.energy.2015.11.021

44. Ma L, Lu Z, Zhang J, Liang R (2010) Thermal performance analysis of the glass evacuated tube solar collector with U-tube. Build Environ 45:1959–1967. https://doi.org/10.1016/j.buildenv.2010.01.015

45. Verma SK, Tiwari AK, Chauhan DS (2016) Performance augmentation in flat plate solar collector using MgO / water nanofluid. Energy Convers Manag 124:607–617. https://doi.org/10.1016/j.enconman.2016.07.007

46. Li Y, Xie HQ, Yu W, Li J (2011) Investigation on Heat Transfer Performances of Nanofluids in Solar Collector. Mater Sci Forum 694:33–36. https://doi.org/10.4028/www.scientific.net/MSF.694.33

47. https://www.mgm.gov.tr/kurumsal/istasyonlarimiz.aspx?sSirala=AL&m=KARABUK, Internet Meteoroloji Genel Müdürlüğü "Dış Saha Ölçümleri". (2016). https://www.mgm.gov.tr/kurumsal/istasyonlarimiz.aspx?sSirala=AL&m=KARABUK

48. European Nuclear Society. Available at: http://www.euronuclear.org/info/encyclopedia/n/nuclear-power-plant-europe.htm, (2017)

49. http://ec.europa.eu/eurostat/statistics-explained/index.php/Electricity_price_statistics, (2016)

50. http://www.worldatlas.com/articles/electricity-rates-around-the-world.html, (2017)